Ultra-high sensitivity graphene photosensors

Ya-Ping Hsieh, Chih-Han Yen, Po-Shin Lin, Shao-Wei Ma, Chu-Chi Ting, Chih-I Wu, and Mario Hofmann

Articles you may be interested in

Highly sensitive wide bandwidth photodetectors using chemical vapor deposited graphene
Appl. Phys. Lett. **104**, 161902 (2014); 10.1063/1.4872267

Sensitivity analysis of single-layer graphene resonators using atomic finite element method
J. Appl. Phys. **114**, 123506 (2013); 10.1063/1.4823735

Quantum mechanical simulation of graphene photodetectors
J. Appl. Phys. **112**, 084316 (2012); 10.1063/1.4759369

Top illuminated inverted organic ultraviolet photosensors with single layer graphene electrodes
Appl. Phys. Lett. **101**, 033302 (2012); 10.1063/1.4733299

Enhanced photosensitivity of electro-oxidized epitaxial graphene
Appl. Phys. Lett. **98**, 093115 (2011); 10.1063/1.3562316

Ultra-high sensitivity graphene photosensors

Ya-Ping Hsieh,[1,a)] Chih-Han Yen,[1] Po-Shin Lin,[1] Shao-Wei Ma,[1] Chu-Chi Ting,[1] Chih-I Wu,[2] and Mario Hofmann[3]

[1]*Graduate of Institute of Opto-Mechatronics, National Chung Cheng University, Chia-yi 62102, Taiwan*
[2]*Department of Electrical Engineering, National Taiwan University, Taipei 10601, Taiwan*
[3]*Department of Material Science and Engineering, National Cheng Kung University, Tainan 70101, Taiwan*

Graphene's advantages for sensor applications are offset by its low electric impedance and consequently low signal-to-noise ratio. We have improved the sensitivity of graphene based photosensors by integrating an energy filtering barrier as an amplifying element. The resulting graphene devices exhibit the highest reported photosensitivity ($I_{on}/I_{off} \sim 4000$, gain ~ 10 A/W) while retaining broad band detection and high speed response. In addition to this unprecedented photosensitivity, the proposed device structure renders the complete graphene photosensitive which enables large scale and flexible photodetectors. The presented approach represents a universal route to enhancing the performance of graphene sensors. © 2014 AIP Publishing LLC.
[http://dx.doi.org/10.1063/1.4863441]

Graphene, a two-dimensional carbon allotrope, has been heralded as an enabling material for sensor applications. Many types of sensors are sharing the same basic operating mechanism in which the sensor stimulus is transduced into a change of electrical properties, such as conductance. Graphene's high mobility and low intrinsic carrier concentration allow the electrical measurement of these sensor stimuli with low noise and high gain. Consequently, applications of graphene as high sensitivity gas sensors,[1] biosensors,[2] strain sensors,[3] and chemical sensors[4] have been reported.

The described advantages, however, are offset by the inherently low impedance of graphene based sensors. Due to graphene's metallic conduction, the transduced electronic signal is overwhelmed by the response from intrinsic carriers. This behavior results in a low signal-to-noise ratio of graphene-based sensors that makes complex amplification schemes necessary.[5] Also, graphene's low impedance results in large driving currents and complicated signal conversion circuits.

Graphene-based photosensors can illustrate this drawback. Graphene is a promising material for photosensors due to its broadband sensitivity[6] caused by its continuous density of states. In addition, graphene's mechanical flexibility and transparency afford the vision of innovative types of photosensors in wearable or implantable devices.[7] The application of graphene to photosensors is impeded by its small intrinsic photocurrent gain and the described low photosensitivity. Consequently, modest gains of 6 mA/W and on/off current ratios of 1% have been reported for graphene sensors[5] which makes lock-in amplification necessary to identify signal from noise.

Hybrid sensing approaches have been investigated to overcome these issues: Semiconductors,[8] metal interfaces,[5,9] quantum dots,[10–12] and chemical functionalization[6] were added to graphene to increase light absorption or improve exciton separation. These approaches have resulted in on-off current ratios of up to 500 for graphene oxide[8] and ~17 for

reduced graphene oxide,[13,14] and photocurrent gain[11] of up to 26 A/W but they deteriorate graphene's broad band absorption and high speed response.[6,8,11,13,14]

We here propose a universally applicable approach to improving the sensitivity of graphene based sensors without changing the sensor operation itself. An element with an energy-selective carrier transmission is added in series to the graphene sensor to amplify small changes in average carrier energy into a larger overall response of graphene sensors. A simple example for such an energy-selective element is a diode in which a junction acts as a high-pass energy filter. Connecting a diode element in series with a graphene resistor, will translate a small change of the graphene resistance into an exponential increase of overall resistance.

In this article, a graphene photosensor is combined with a dielectric barrier acting as the non-linear element. Proof-of-concept devices exhibit an increased sensitivity of more than 3 orders of magnitude and an improvement in gain of 4 orders of magnitude.[5] These values for photosensitivity and photocurrent gain are the highest reported values for graphene or graphene-hybrid devices. Finally, a uniform photoresponse of CVD graphene derived photosensors was observed that enables large area photosensors for future applications.

Graphene/barrier devices were produced by first fabricating a barrier on a Cu substrate and subsequent chemical vapor deposition of graphene. The Cu foil substrate was pretreated by electrochemical polishing to ensure high smoothness.[15] A lateral dielectric barrier was formed on the Cu foil by oxidation of a strip of thermally evaporated aluminum. The formed aluminum oxide is known to suppress graphene formation on Cu foil and also acts as an insulating barrier for carrier transport.[16] Graphene was then grown on the thus prepared substrate under low pressure using methane following previous reports.[17] The produced graphene/barrier film was then transferred onto SiO_2 substrates by spinning a thin layer of Polymethylmethacrylate (PMMA) and chemically removing the Cu substrate.[18]

First, the photoresponse of pristine graphene was investigated. In this case, the dark-current is of similar magnitude as

---

a)Author to whom correspondence should be addressed. Electronic mail: yphsieh@ccu.edu.tw.
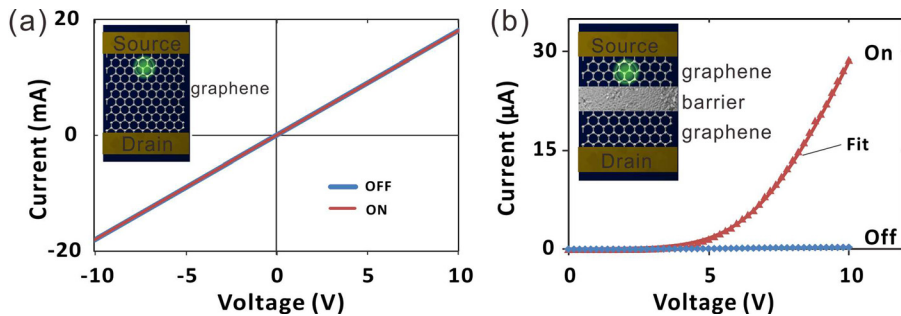
FIG. 1. Photoresponse of (a) pristine graphene, (b) graphene/barrier device, (insets) schematics of device structures.

the device current under illumination (Fig. 1(a)) which is expected from low impedance devices. The photosensitivity, as expressed by the light-to-dark-current ratio, is only approximately 1% of the total current. These observations agree with previous reports of graphene-based photosensors.[6,10]

Measuring the photocurrent response of graphene in series with an Aluminum oxide barrier reveals a very different result. Instead of a linear relation between current and voltage, as seen in the pristine graphene devices (Fig. 1(a)), a pronounced non-linear current-voltage (I-V) curve is observed as shown in Fig. 1(b). This behavior and the increase in device impedance by 3 orders of magnitude are attributed to the added dielectric barrier that impedes current transport.

Furthermore, a significant difference between current amplitude under dark and light conditions is found (Fig. 1(b)). The on-off ratio of the shown device is approximately 100 at 10 V and, upon optimization, devices with sensitivities up to 4000 were measured. These values represent the highest reported photosensitivity of graphene based photosensors to date and warrant a detailed investigation of the enhancement mechanism.

The non-linear I-V characteristics of the graphene/barrier device (Fig. 1(b)) is dominated by the carrier transmission across the barrier. Upon illumination, a number of photoexcited carriers are generated within the graphene which changes the material's Fermi level. Consequently, an apparent decrease in barrier height occurs for the excited case. The larger number of electrons able to surmount the barrier causes an increase in photocurrent.

The thermionic emission model can be applied to extract the barrier height change under illumination using Eq. (1), where A* is the Richardson constant, ϕ_B is the barrier height, and V_T is the thermal voltage

$$J = A^* A T^2 \exp(-\Phi_B/V_T)(\exp(V/V_T) - 1). \quad (1)$$

Good agreement of the data with the fit to the described model can be seen after accounting for a series resistance stemming from the graphene contacts. Due to the absence of reliable values for cross sectional area and the Richardson constant of the graphene/alumina junctions, the extracted 0.58 eV barrier height can only serve as an approximation. To better quantify the barrier height, Ultraviolet Photoelectron Spectroscopy (UPS) was carried out (Fig. 2(a)). Work functions for graphene and aluminum were measured to be 4.35 eV and 3.95 eV, respectively. These values are in agreement with previous reports[20] and the work function difference agrees

qualitatively with the estimated barrier height from electrical measurements.

The proposed model (illustrated in Fig. 2(b)) suggests that the number of photoexcited carriers, and consequently the Fermi level, will depend on the illumination power. To confirm this hypothesis, we conducted power dependent I-V measurements to characterize the change in barrier height. Indeed, a decrease of the apparent barrier height due to a photoinduced increase of the graphene Fermi level is observed (Fig. 2(d)). At higher laser powers, current saturation occurs (Fig. 2(c)). This is attributed to the increased recombination efficiency at higher photocarrier concentration.

To further elucidate the operation mechanism, photocurrent was measured as a function of illumination location on the sample. A bias was applied to two graphene sides in contact with an alumina barrier. Upon weak biasing (1 V/mm), we observed that only the negatively biased graphene side was generating a photocurrent. From this selectivity, it can be inferred that the current is carried by electrons across the barrier. This observation is in agreement with the predicted band alignment of graphene and aluminum oxide which would have a significantly lower barrier for electron injection than hole injection.

The photocurrent map (Fig. 3(a)) furthermore reveals an unusually large photoresponse (1 A/W @ 532 nm excitation)
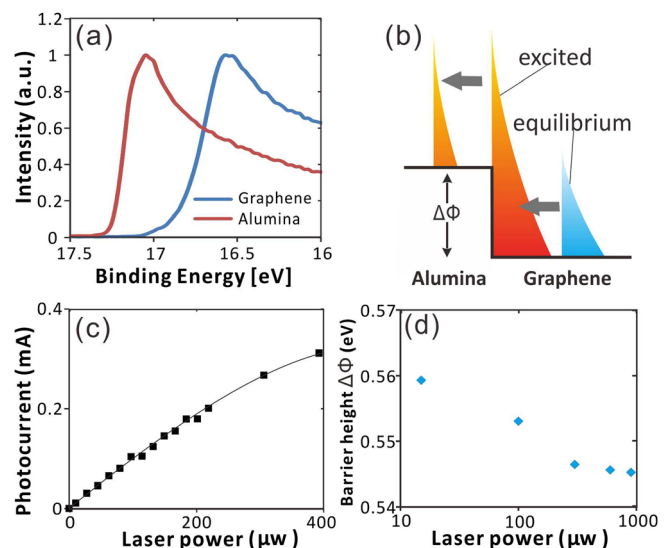

FIG. 2. (a) UPS spectrum of secondary emission onset of graphene and barrier region, (b) schematic of device operation, (c) power dependence of photocurrent under 532 nm excitation, and (d) change of extracted barrier height under illumination.
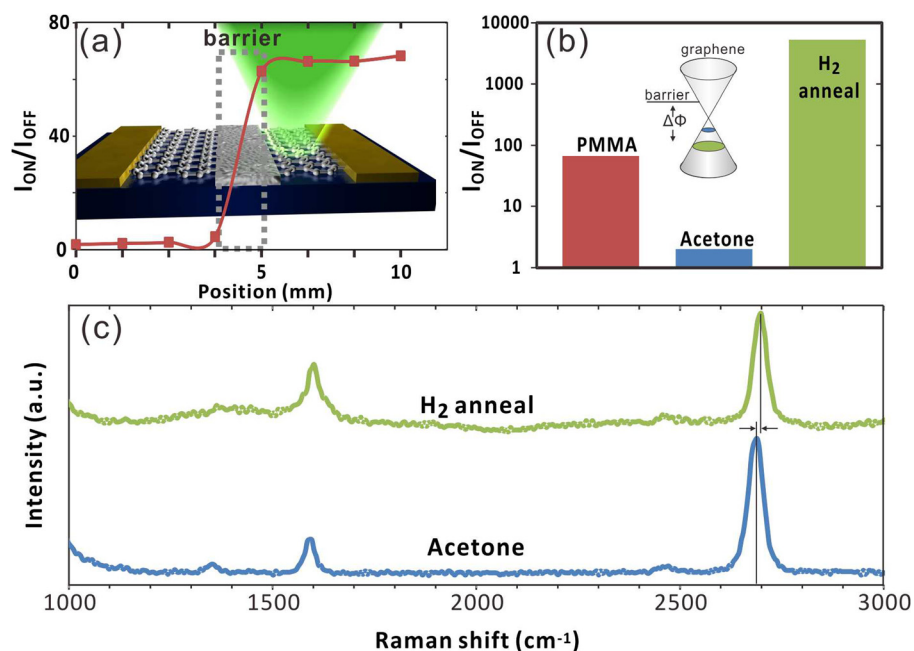
FIG. 3. (a) Position dependence of on/off current ratio within graphene/barrier device under 532 nm excitation, (b) change of photoresponse before and after PMMA removal using immersion in acetone or annealing under H_2, (inset) schematic of changes to band alignment due to doping, and (c) Raman spectra of graphene after either route of PMMA removal with indication of G'-band shift.

that occurs uniformly across the entire graphene area (∼up to 1 cm^2). This behavior is different from traditional graphene photosensors, where large fields associated with contacts and interfaces are required to dissociate photogenerated electrons and holes. The observed large extent of the photosensitive region and the uniform photosensitivity of our graphene devices indicate that the graphene itself produces the photoresponse. This photosensing mechanism is expected from the proposed barrier device and was investigated by changing the graphene properties. Commonly, a thin PMMA membrane is used to protect the graphene film during transfer from the growth substrate to a target substrate and then removed.[19] We observed a marked change in photoresponse depending on the PMMA removal protocol (Fig. 3(b)). If the sample was rinsed with acetone, following previous reports,[21] the on-off ratio decreased during the removal process. On the other hand, if a high temperature PMMA removal step under Argon and Hydrogen, following Ref. 22, was used, the photoresponse increased by one order of magnitude (up to I_{on}/I_{off} ∼ 4000).

Previously, high temperature treatment of PMMA on graphene was associated with the formation of covalent bonds and morphological defects in graphene.[23] Indeed, Raman spectra (Fig. 3(c)) exhibit a broad background around the defect-related D-band (1350 cm^{-1}) upon hydrogen treatment in agreement with previous reports.[23] These defects can act as charge traps[24] and cause additional p-type doping of the graphene. We conducted Hall-effect measurements in van-der-Pauw geometry and observed an increase in hole density from 1.8×10^{12}cm^{-2} for acetone removal to 7.3×10^{12}cm^{-2} for H_2 annealing. This doping results in lowering of the Fermi level by 0.16 eV which is in excellent agreement with the Fermi level shift extracted from the shift of the double-resonant Raman G'-feature.[25]

The lowering of the Fermi-level affects the energy required for carriers to surmount the dielectric barrier. Fitting of the current-voltage characteristics indeed showed that devices exposed to acetone exhibited a barrier that was 0.15 eV higher compared to devices subjected to hydrogen annealing. We therefore conclude that the photosensitivity of barrier devices is very sensitive to the Fermi-level of the graphene which agrees with our previous model. Light induced changes to the Fermi-level would propagate throughout the graphene device and carrier transmission at the graphene/barrier interface can be enhanced. This property results in the contribution of the entire graphene film to the photosensing process and barrier devices could be applied as large scale uniform photodetectors for future sensor applications such as flexible detectors, large scale imaging, and transparent cameras.

The presence of the described trap states will not affect the light absorption behavior of graphene in the visible range since they are expected to be at low energy compared to optical excitation energies. Therefore, the broad band sensitivity of graphene should be retained for wavelength shorter than at least 2 μm.

We investigated the spectral photosensitivity of graphene over a wavelength range from 200 to 700 nm (Fig. 4(a)) and the predicted broad band sensitivity was confirmed. The high UV sensitivity (up to 12 A/W at UV at 260 nm) is attributed to an increased absorption of the graphene in this range due to maxima in its density of states. The increase in IR photoresponse could be due to resonance effects with the adsorbed functional groups or trap states that enhance absorption. Even in the lowest spectral sensitivity region around 450 nm the graphene sensors still exhibit a sensitivity of 0.5 A/W, which is approximately 2 orders of magnitude higher than previously reported values.[5]

The speed of the photoresponse was investigated through time-resolved photocurrent measurements (Fig. 4(b)). The observed response time of approximately 150 μs rules out photothermal effects as reported in graphene oxide devices.[14] The measured time agrees with estimates for the transition time of an electron through the used 1 cm graphene device based on measured device dimensions, voltage, and CVD graphene carrier mobility. We therefore anticipate significant
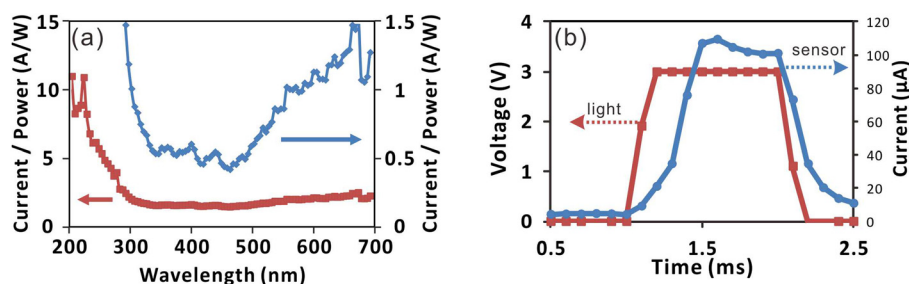
FIG. 4. (a) Spectral photosensor gain on large scale (left) and higher resolution scale (right) (b). Photoresponse under pulsed illumination.

increase of the device performance upon decrease of the sensor dimensions for high-speed detection applications.

Due to the absence of an excitation energy dependence, the operation mechanism seems to not be related to the generation of photoexcited carriers that surmount the barrier. Instead the photoinduced increase in carrier density and trapping of minority carriers shifts the Fermi level of the majority carriers (Fig. 2(b)). Their larger average energy results in a larger fraction of carriers being able to surmount the barrier. Therefore, an exponential relation between Fermi level change and carrier transmission exists which represents the working principle of the graphene/barrier device. Consequently, an estimate of the device performance can be made from Eq. (1). The on/off current ratio will depend on the number of carriers (n) in graphene, the thermal voltage (V_T), and the number of added carriers during sensor operation (Δn) according to Eq. (2), where ν_F is the Fermi velocity in graphene

$$\frac{I_{on}}{I_{off}} = \exp\left[\frac{-h\nu_F\left(\sqrt{n + \Delta n} - \sqrt{n}\right)}{V_T}\right]. \quad (2)$$

Thus, the low intrinsic carrier density of graphene at the Dirac point and its high Fermi velocity make graphene ideally suited for the described approach for high sensitivity device operation.

This mechanism is expected to be compatible with any stimulus that changes the Fermi level, which makes the sensing mechanism universal and applicable to many types of chemical and optoelectronic sensors. Furthermore, the increased device impedance lowers the power consumption of graphene sensors significantly which can aid the implementation of graphene sensors in mobile devices. Also, the large device impedance simplifies the integration of graphene sensors into existing electronic circuits without the need for converter stages.

The device operation is anticipated to be robust since the height of the used barrier is only affecting the device impedance and not the sensing mechanism. That is to say, any barrier height in excess of the thermal energy of carriers will produce a sensitivity increase of graphene based sensors. Consequently, a wide variety of barriers can be envisioned that can improve the performance of graphene sensor devices.

The presented mechanism is also not limited to dielectric barriers. Any energy dependent filtering of carriers would result in a similar amplification scheme. As an example, Schottky barriers, which are occurring at metal/graphene or semiconductor/graphene junction would be suitable

non-linear elements. Therefore, a careful choice of contacts can increase the sensitivity of graphene based sensors.[26]

In conclusion, we demonstrated a universally applicable approach for improving the sensor response of graphene devices such as gas sensors, chemical sensors, etc. An element with energy-selective carrier transmission, in the form of a barrier, was introduced into a graphene photosensor and a significant increase in device sensitivity was observed. This sensing process was found to render the complete graphene device photosensitive. Finally, the demonstrated broad band sensitivity, large scale compatibility, and high speed afford the vision of graphene based sensors for future applications.

[1]F. Schedin, A. K. Geim, S. V. Morozov, E. W. Hill, P. Blake, M. I. Katsnelson, and K. S. Novoselov, Nature Mater. **6**, 652 (2007).
[2]K. F. Zhou, Y. H. Zhu, X. L. Yang, J. Luo, C. Z. Li, and S. R. Luan, Electrochim. Acta **55**, 3055 (2010).
[3]A. Sakhaee-Pour, M. T. Ahmadian, and A. Vafai, Solid State Commun. **147**, 336 (2008).
[4]J. D. Fowler, M. J. Allen, V. C. Tung, Y. Yang, R. B. Kaner, and B. H. Weiller, ACS Nano **3**, 301 (2009).
[5]T. Mueller, F. N. A. Xia, and P. Avouris, Nat. Photonics **4**, 297 (2010).
[6]M. E. Itkis, F. H. Wang, P. Ramesh, E. Bekyarova, S. Niyogi, X. L. Chi, C. Berger, W. A. de Heer, and R. C. Haddon, Appl. Phys. Lett. **98**, 093115 (2011).
[7]I. W. Jung, J. L. Xiao, V. Malyarchuk, C. F. Lu, M. Li, Z. J. Liu, J. Yoon, Y. G. Huang, and J. A. Rogers, Proc. Natl. Acad. Sci. U. S. A. **108**, 1788 (2011).
[8]K. K. Manga, S. Wang, M. Jaiswal, Q. Bao, and K. P. Loh, Adv. Mater. **22**, 5265 (2010).
[9]M. C. Lemme, F. H. Koppens, A. L. Falk, M. S. Rudner, H. Park, L. S. Levitov, and C. M. Marcus, Nano Lett. **11**, 4134 (2011); A. Urich, K. Unterrainer, and T. Mueller, *ibid.* **11**, 2804 (2011); F. Xia, T. Mueller, R. Golizadeh-Mojarad, M. Freitag, Y. M. Lin, J. Tsang, V. Perebeinos, and P. Avouris, *ibid.* **9**, 1039 (2009).
[10]X. Geng, L. Niu, Z. Xing, R. Song, G. Liu, M. Sun, G. Cheng, H. Zhong, Z. Liu, Z. Zhang, L. Sun, H. Xu, L. Lu, and L. Liu, Adv. Mater. **22**, 638 (2010).
[11]D. Zhang, L. Gan, Y. Cao, Q. Wang, L. Qi, and X. Guo, Adv. Mater. **24**, 2715 (2012).
[12]H. Chang, Z. Sun, K. Y. Ho, X. Tao, F. Yan, W. M. Kwok, and Z. Zheng, Nanoscale **3**, 258 (2011).
[13]H. Liang, W. Ren, J. Su, and C. Cai, Thin Solid Films **521**, 163 (2012).
[14]Y. Lin, K. Zhang, W. Chen, Y. Liu, Z. Geng, J. Zeng, N. Pan, L. Yan, X. Wang, and J. G. Hou, ACS Nano **4**, 3033 (2010).
[15]Z. Luo, Y. Lu, D. W. Singer, M. E. Berck, L. A. Somers, B. R. Goldsmith, and A. T. Charlie Johnson, Chem. Mater. **23**, 1441 (2011).
[16]M. Hofmann, Y.-P. Hsieh, A. L. Hsu, and J. Kong, Nanoscale **6**, 289 (2014).
[17]M. Hofmann, Y. C. Shin, Y. P. Hsieh, M. S. Dresselhaus, and J. Kong, Nano Res. **5**, 504 (2012).
[18]See supplementary material at http://dx.doi.org/10.1063/1.4863441 for details on the fabrication process.

[19]S. Das, P. Sudhagar, E. Ito, D.-y. Lee, S. Nagarajan, S. Yun Lee, Y. Soo Kang, and W. Choi, J. Mater. Chem. **22**, 20490 (2012).

[20]X. S. Li, Y. W. Zhu, W. W. Cai, M. Borysiak, B. Y. Han, D. Chen, R. D. Piner, L. Colombo, and R. S. Ruoff, Nano Lett. **9**, 4359 (2009).

[21]W. Regan, N. Alem, B. Aleman, B. S. Geng, C. Girit, L. Maserati, F. Wang, M. Crommie, and A. Zettl, Appl. Phys. Lett. **96**, 113102 (2010).

[22]J. Rafiee, X. Mi, H. Gullapalli, A. V. Thomas, F. Yavari, Y. F. Shi, P. M. Ajayan, and N. A. Koratkar, Nature Mater. **11**, 217 (2012).

[23]Y. C. Lin, C. C. Lu, C. H. Yeh, C. Jin, K. Suenaga, and P. W. Chiu, Nano Lett. **12**, 414 (2012).

[24]M. J. Allen, V. C. Tung, and R. B. Kaner, Chem. Rev. **110**, 132 (2010).

[25]A. Das, S. Pisana, B. Chakraborty, S. Piscanec, S. K. Saha, U. V. Waghmare, K. S. Novoselov, H. R. Krishnamurthy, A. K. Geim, and A. C. Ferrari, Nat. Nanotechnol. **3**, 210 (2008).

[26]H. Y. Kim, K. Lee, N. McEvoy, C. Yim, and G. S. Duesberg, Nano Lett. **13**, 2182 (2013).